行政院國家科學委員會專題研究計畫　期中進度報告

子計畫五：鈣鈦礦結構磁性金屬氧化物薄膜之相分離與晶界磁電阻特性與關係研究(2/3)

計畫類別： 整合型計畫
計畫編號： NSC93-2112-M-009-017-
執行期間： 93 年 08 月 01 日至 94 年 07 月 31 日
執行單位： 國立交通大學電子物理學系(所)

計畫主持人： 溫增明

計畫參與人員： 張維仁、蔡於璁

報告類型： 精簡報告

處理方式： 本計畫可公開查詢

中　華　民　國 94 年 5 月 30 日

行政院國家科學委員會補助專題研究計畫 □ 成 果 報 告 ☑期中進度報告

過渡金屬氧化物薄膜物理與元件研究-子計畫五：鈣鈦礦結構磁性金屬氧化物薄膜之相分離與晶界磁電阻特性與關係研究(2/3)

計畫類別：□ 個別型計畫　☑ 整合型計畫
計畫編號：NSC 93－2112－M－009－017－
執行期間：2004 年 08 月 01 日至 2005 年 07 月 31 日

計畫主持人：溫增明
共同主持人：
計畫參與人員：張維仁、蔡於璁

成果報告類型(依經費核定清單規定繳交)：☑精簡報告　□完整報告

本成果報告包括以下應繳交之附件：
□赴國外出差或研習心得報告一份
□赴大陸地區出差或研習心得報告一份
□出席國際學術會議心得報告及發表之論文各一份
□國際合作研究計畫國外研究報告書一份

處理方式：除產學合作研究計畫、提升產業技術及人才培育研究計畫、列管計畫及下列情形者外，得立即公開查詢
□涉及專利或其他智慧財產權，□一年□二年後可公開查詢

執行單位：國立交通大學電子物理學系(所)

中　華　民　國　94 年　05 月　31 日

中文摘要:

關鍵詞：穿隧掃瞄電子顯微鏡、相分離、四價參雜、x 光吸收光譜、LDA+*U* 計算

我們利用穿隧掃瞄電子顯微鏡觀察到 $La_{0.7}Ca_{0.3}MnO_3$ 與 $La_{0.7}Ce_{0.3}MnO_3$ 皆具有奈米尺度的相分離現象。藉由將相分離的影像以直方圖來做統計，我們可以很清楚的看出相分離現象在 LCaMO 與 LCeMO 中隨溫度的演進。為了更進一步瞭解 LCeMO 的電子結構，我們做了 x 光吸收光譜的實驗。結果顯示 LCeMO 的空軌域確實比 LCaMO 來的少，也就是說電子確實有參雜進入 e_g 能帶。這結果也與 LDA+*U* 的計算結果相符。

Abstract:

Key words: STM, phase separation, tetravalent-doped, XAS, LDA+*U* calculation.

We used the scanning tunneling spectroscopy (STM) image technique to observe evidence of nanoscale phase separation in the divalent-doped $La_{0.7}Ca_{0.3}MnO_3$ thin films (LCaMO) at various temperatures. In this report, we will present the results of the scanning tunneling spectra (STS) and spectroscopic images obtained in the tetravalent-doped $La_{0.7}Ce_{0.3}MnO_3$ thin films (LCeMO). The results show that, similar to the divalent-doped compounds, the phase separation starts to emerge in the vicinity of the transition temperature. The evolution of the separating phase as a function of temperature is clearly demonstrated in the histogram. Further, x-ray absorption spectroscopy (XAS) was used to investigate the electronic structure in LCeMO. The results of XAS are consistent with those from LDA+*U* calculations in that the doping of Ce has shifted up the Fermi.

Introduction:

Over the last decade, researches on the rare-earth manganese perovskites, $RE_{1-x}A_xMnO_3$ (RE: rare-earth ion, A: alkaline earth cation), have been largely devoted to the characteristics related to the electric transport and magnetic properties, e.g., colossal magnetoresistance, phase separation, and the competition between the charge, spin, and orbital order parameter [1]. In these compounds, the charge state of Mn displays a mixed valence characteristic of Mn^{3+} and Mn^{4+}, and the ratio of Mn^{3+}/Mn^{4+} depends strongly on the doping level of the divalent cation. Intuitively, substituting the divalent cation with the tetravalent cation, such as Ce, Sn, etc., should impel the valence state of Mn to a mixed-valent state of Mn^{2+} and Mn^{3+} [2, 3]. It then raises curiosities on how the electric transport and magnetic properties of tetravalent cation doped manganites would prevail, as compared with the divalent-doped system.

Previously, the transport properties and the electronic structure of LCeMO had been reported with results obtained from the tunneling junction, photoemission, and XAS experiments [5-9]. The results showed that the valance state of Mn is indeed a mixed valence of Mn^{2+}/Mn^{3+}, and it's probably electron-doped. However, there are discrepancies among the reported results. For instance, the tunneling junction experiments suggested that the itinerant carriers in LCeMO are the minority spin carriers [5], which was in sharp contrast to the conclusion of the majority spin carriers drown from XAS experiments and theoretical calculations [9, 10]. Our results unambiguously clarified some of the outstanding controversies in this system.

Experiments:

STM were used to obtain surface topographic and spectroscopic images at constant current mode with $Pt_{0.8}Ir_{0.2}$ tip simultaneously. LCeMO and LCaMO were both biased at 0.7 V relative to tip potential and the tunneling current were set at 0.5 and 0.2 nA, respectively. The lock-in amplifier was used in the measurements of spectroscopic images as a standard lock-in technique [4]. The lock-in amplifier applied a small-modulating signal on bias voltage (<3% bias voltage) and sensed the modulated-tunneling current to output differential conductivity (dI/dV) data during scanning. STM was operated at slow-scanning rate in acquiring images to improve the resolution of spectroscopic images, and the dI/dV signal from lock-in amplifier were recorded with z-axis signal simultaneously. To choose a scanning area of spectroscopic images, the maximum depth of topography, peak to valley, is smaller then 20 nm in order to avoid turbulent tunneling current.

Details of preparing the single phase LCeMO on (100) $SrTiO_3$ substrates by pulsed-laser deposition and the associated structure-property analyses were reported in Ref. [11]. The x-ray scattering and x-ray diffraction results indicated that the obtained LCeMO films were highly epitaxial single-phase samples with negligible traces of impurity phases like CeO_2 and MnO. The O *K*-edge and Mn *L*-edge XAS spectra were carried out using linear polarized synchrotron radiation from 6-m high-energy spherical grating monochromator beamline located at NSRRC in Taiwan. Details of XAS experiments can be found in Ref. [12]. Being different from previous XAS measurements at 300 K [7-9], the O 1*s* XAS spectra of LCeMO and LCaMO were taken by x-ray fluorescence yield at 30 K, which directly probed the electronic structure in the ferromagnetic state for both samples. The band structure calculations were performed using the

full-potential projected augmented wave method [13] as implemented in the Vienna *ab initio* simulation package (VASP) [14] within the local-density approximation plus on-site Coulomb interaction U (LDA+U) scheme [15]. In the LDA+U calculations, we used Coulomb energy U=5.0 eV and exchange parameter J=0.95 eV for Ce(La)-4f electrons, while U=4.0 eV and J=0.87 eV were used for Mn-3d electrons [9].

Results & Discussion:

We had measured STS and spectroscopic images over a wide temperature range, which covered both of paramagnetism and ferromagnetism. In most regions of surfaces, the metal-insulator separations were not wholly relative to topography but some extremely steep relief on surface, grain boundaries, shut off the drift of metallic phase at ravines. As shown in Fig. 1, there are some small dark regions (more metallic) in spectroscopic images of LCeMO at 300 K. Although the dark regions show more metallic states to the other regions at 300 K, the non-linear I-V characteristics are considerably insulating for these darker regions. At the hillside of ρ-T curves, 230 and 250 K for LCeMO and LCaMO respectively, there are some tarnished patterns whereas both have obvious phase separation at 80 K.

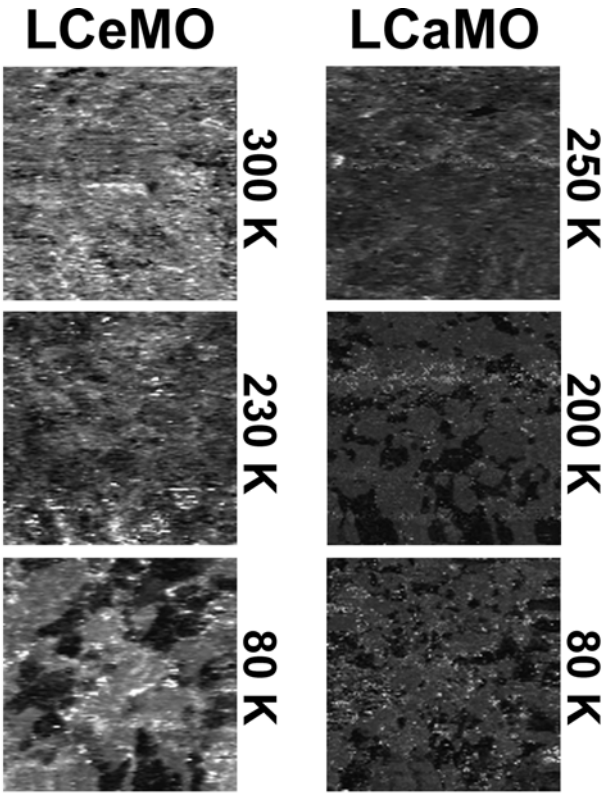

FIG. 1

In Fig. 2, it's clear to observe the phenomenon of phase separation by collating the histograms. The spectroscopic signature of LCaMO displayed the separated patterns of insulated and metallic phase at 200 K, but not in LCeMO, and the high contrast of metallic and insulating state reveals until cooling down below 200 K. The evident phase separation of LCaMO at 200 K demonstrates sharp drop of resistivity around metal-insulator transition than of LCeMO. At 200 K, LCaMO shows the marked separation in histogram and obvious-large dark regions in spectroscopic image, as shown in Fig. 1 & 2, and whole states convert into metallic state with decreasing temperature.

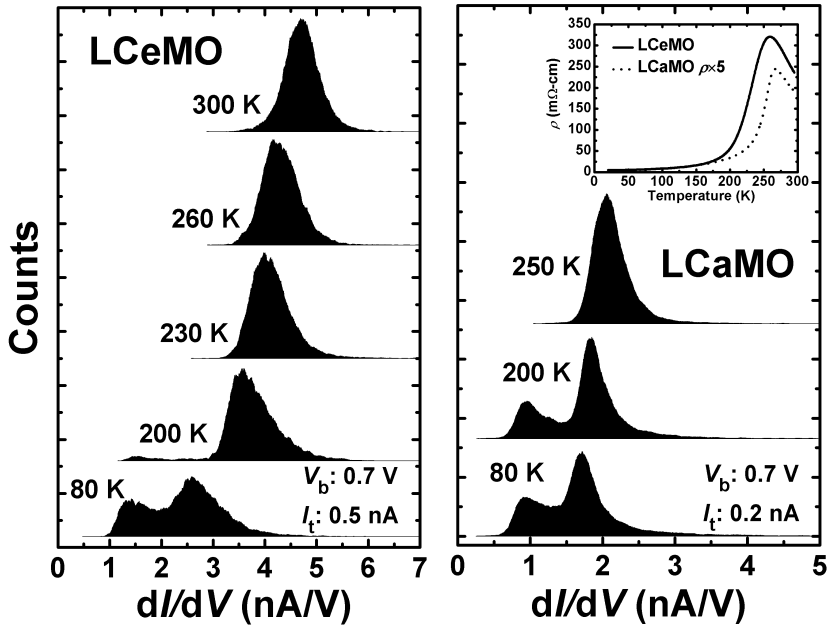

FIG. 2

Although the average values of d*I*/d*V* decrease with the decrease of temperature in LCeMO, the apparent segregation has been observed until at 80 K, which is much different from LCaMO. However, both are similar in the evolution of metallic and insulating states. Below T_C, the amount of metallic states, around 1.5 and 1.0 nA/V for LCeMO and LCaMO respectively, increase with decreasing temperature, but insulating states shift to smaller d*I*/d*V* value with the decrease of temperature. These indicate that the metal-insulator transition, explicated by percolation theory, results from the growth of metallic states, and the decreasing resistivity with temperature above 80 K, residual resistivity, and ferromagnetism transition are dominated by the evolution of insulating states. In the full ferromagnetism, the electronic transport properties below 80 K are dominated by residual resistivity, two-magnon scattering, and small-polaron coherent motion [16]. The origin of different behaviors in phase separation between LCeMO and LCaMO may be due to the variety of their average ionic radius of A site and the different e_g band structure from tetravalent and divalent cation doping [17].

To characterize the valence state of manganese in LCeMO, Mn *L*-edge XAS spectra of MnO_2, Mn_2O_3, MnO, LCaMO, and LCeMO were measured and are shown in Fig. 3(a) for comparison. The spectral weight of Mn *L*-edge for LCeMO evidently exhibits the characteristics of both Mn^{2+} and Mn^{3+}, which has been previously interpreted as manifestations of Mn^{2+}/Mn^{3+} mixed-state in LCeMO [7-8]. In Fig. 3(b), O *K*-edge XAS spectrum of LCeMO reveals a shoulder near absorption edge as compared with the first pronounced peak of LCaMO at 529 eV. These results suggest that there are fewer unoccupied states in $e_g\uparrow$ band of LCeMO than in that of LCaMO due to extra electrons doped into the e_g band of LCeMO, presumably originated from substituting Ca^{2+} with Ce^{4+}. Based on these XAS results, the electronic structure of LCeMO appears to be consistent with the scenario of the majority spin carriers associated with strong Hund's rule effects. On the other hand, for the minority spin scenario to prevail one would expect otherwise a strong O *K*-edge spectral weight in the vicinity of the absorption edge. The electronic structure diagrams for the scenarios discussed above are depicted schematically in Fig. 3 (c). The density of states spectra obtained from LDA+*U* calculations (Fig. 4) also revealed that both

LCeMO and LCaMO are majority spin half-metals with fewer unoccupied $e_g\uparrow$ states in LCeMO. This is in good agreement with the observed XAS spectra mentioned above. The above analyses unambiguously demonstrate that electrons are indeed doped into LCeMO. Moreover, as displayed in the inset of Fig. 3(b), the mixed-valence Mn^{2+}/Mn^{3+} also leads to typical magneto-transport properties of CMR manganites, with T_c and T_{IM} being around 260 K, which is also consistent with most of the previous reports [3-9].

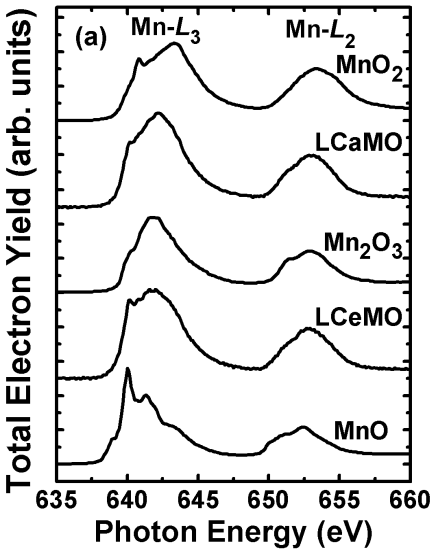

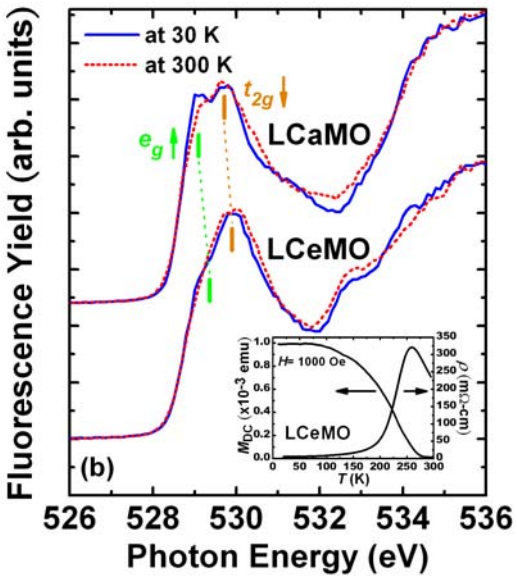

FIG. (a)(b)

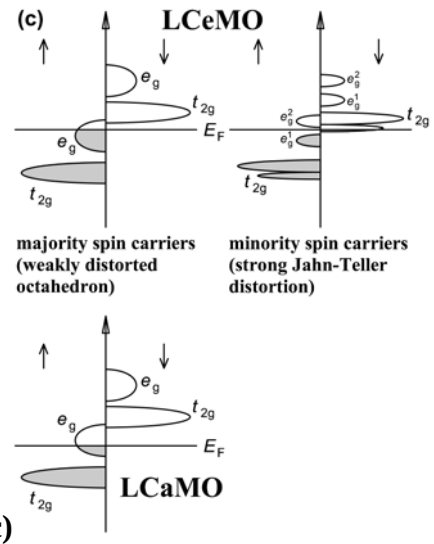

FIG. 3(c)

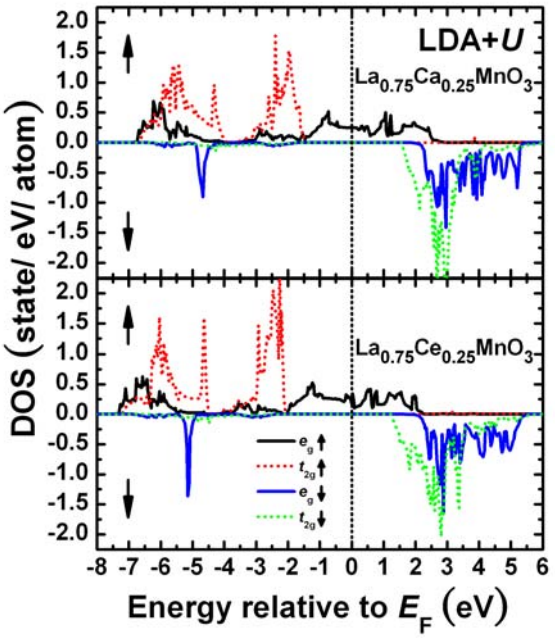

FIG. 4

Conclusion:

In summary, we had measured the STS and spectroscopic images of LCeMO and LCaMO from 300 K to 80 K. Beside the similar ρ-T, M-T transition, and transport carriers of e_g band, the

results show that phase separation coexist in divalent-doped and tetravalent-doped compounds, which can be observed clearly in the histograms of spectroscopic images. In addition, LCaMO reveals contrastive segregation of metallic state under T_C compared with LCeMO, and the relation between insulating state and temperature corresponds to the behavior of ρ-T qualitatively. We also have presented the detailed results of Mn L-edge and O K-edge XAS which suggest that LCeMO is a majority spin carrier ferromagnet. The results also display clear evidence of electron-doping into the $e_g\uparrow$ sub-band of LCeMO.

Reference:

[1] M. Imada, A. Fujimori, and Y. Tokura, Rev. Mod. Phys. **70**, 1039 (1998); E. Dagotto, T. Hotta, and A. Moreo, Phys. Rep. **344**, 1 (2001).

[2] P. Raychaudhuri *et al*., J. Appl. Phys. **86**, 5718 (1999).

[3] Z. W. Li, A. H. Morrish, and J. Z. Jiang, Phys. Rev. B **60**, 10284 (1999).

[4] S. F. Chen, P. I. Lin, J. Y. Juang, T. M. Uen, K. H. Wu, Y. S. Gou, and J. Y. Lin, Appl. Phys. Lett. **82**, 1242 (2003).

[5] C. Mitra *et al*., Phys. Rev. Lett. **90**, 017202 (2003).

[6] C. Mitra *et al*., Appl. Phys. Lett. **79**, 2408 (2001).

[7] C. Mitra *et al*., Phys. Rev. B **67**, 092404 (2003).

[8] J.-Y. Lin *et al*., J. Magn. Magn. Mater. **282**, 237 (2004).

[9] S. W. Han *et al*., Phys. Rev. B **69**, 104406 (2004).

[10] Q. Zhang and W. Zhang, Phys. Rev. B **68**, 134449 (2003).

[11] W. J. Chang *et al*., J. Appl. Phys. **96**, 4357 (2004).

[12] I. P. Hong *et al*., Europhys. Lett. **58,** 126 (2002); H. D. Yang *et al*., Phys. Rev. B **68**, 092507 (2003).

[13] G. Kresse and D. Joubert, Phys. Rev. B **59**, 1758 (1999).

[14] G. Kresse and J. Furthmüller, Phys. Rev. B **54**, 11169 (1996).

[15] A. I. Liechtenstein, V. I. Anisimov, and J. Zaanen, Phys. Rev. B **52**, R5467 (1995).

[16] G. M. Zhao, V Smolyaninova, W. Prellier, and H. Keller, Phys. Rev. Lett. **84**, 6086 (2000).

[17] W. J. Chang *et al*. (to be published).